

Query No. Query

AQ1 Should
1,5 be
presented as
1.5? Please
check.

Electrochemistry of Copper in
Polyacrylic Acid: [The](#) Electrode
Mechanism and Analytical Application
for Gaseous Hydrogen Peroxide
Detection

Leon Stojanov^{†a},
Angela Rafailovska^{†a},
Vasko Jovanovski^{†b}, [and](#)
Valentin Mirceski^{*†a,§e,¶d*}

^aInstitute of Chemistry, Faculty of Natural Sciences and Mathematics, “Ss Cyril and Methodius” University in Skopje, P.O. Box 162, Skopje 1000, North Macedonia

^bDepartment of Materials Chemistry, National Institute of Chemistry, Hajdrihova 19, Ljubljana 1000, Slovenia

^cDepartment of Inorganic and Analytical Chemistry, University of Lodz, Tamka 12, Lodz 91-403, Poland

^dResearch Center for Environment and Materials, Macedonian Academy of Sciences and Arts, Bul. Krste Misirkov 2, Skopje 1000, North Macedonia

*E-mail: valentin@pmf.ukim.mk

Abstract

Electrode reaction of copper(II) reduction in an aqueous solution of polyacrylic acid (PAA) is studied by means of cyclic staircase and square-wave voltammetry ~~in-order~~ to establish a basis for an electrochemical sensor for gaseous hydrogen peroxide detection. It has been determined that the reduction mechanism at a glassy carbon electrode follows a two-step, consecutive electron transfer reaction scheme of Cu^{2+} to the final copper solid deposit, via the formation of the intermediate Cu^+ ions, which are subject to a fast disproportionation reaction. Experimental data have been supported by theoretical considerations and simulations based on EC'E electrode mechanism, where E designates an electrode reaction, whereas C' is a homogeneous regenerative chemical reaction. Estimated thermodynamic and kinetic data of the electrode mechanism suggest stabilization of the intermediate Cu^+ form by PAA in comparison with a pure aqueous medium. Commercially available screen-printed carbon electrodes were covered with a film of 1% (mass percent) of aqueous PAA solution containing Cu^{2+} ions, which proves to be a promising platform for gaseous H_2O_2 detection, where the $\text{Cu}^{2+}/\text{Cu}^+$ couple serves as a redox mediator for H_2O_2 reduction, with a limit of detection at a sub- $\mu\text{g}\cdot\text{dm}^{-3}$ concentration level in the gas phase.

Keywords:

copper reduction mechanism

voltammetry

electrochemical sensor
gaseous hydrogen peroxide

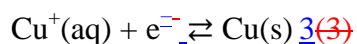
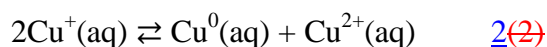
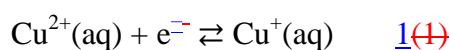
1. Introduction

Polyacrylic acid (PAA) is a well-known polymer and a suitable polyelectrolyte with a broad range of applications,^{1–5} which has attracted notable interest due to superior biocompatibility,^{6–10} perfect water absorptivity, and good thin-film formability.^{11–14} Particular properties of PAA depend strongly on the degree of cross-linking of the polymeric molecules; while significantly cross-linked PAA is water-insoluble, the non-cross-linked form is water-soluble, and the gel phase can be formed under a broad range of pH values. The physicochemical properties of the PAA gel are predominantly controlled by the concentration and the size of polymeric molecules, temperature, ionic strength, the type of the counter ions, etc. The non-cross-linked PAA is partly dissociated in water, and the pK_a value is estimated to be close to 4,¹⁵ the exact value depending on the polymer size (molar mass). The molecular size is also important for the pH-dependent conformational state in an aqueous solution. Commonly, polymeric molecules with a high molar mass ($M_w > 16,000$ g/mol) change their conformation depending on pH.¹⁷

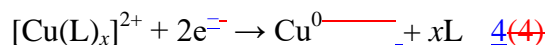
Due to polyelectrolytic features and versatility of physicochemical characteristics, the aqueous PAA gel is an excellent basis for the preparation of electrochemical gas sensors.^{18–20} The motivation of the current study is to use PAA as a medium for gaseous hydrogen peroxide (H_2O_2) electrochemical detection, using copper(II) ions as a redox mediator. Thus, the electrode mechanism of copper(II) reduction in a non-cross-linked PAA aqueous solution at a glassy carbon electrode was studied in detail using cyclic staircase (CSV) and square-wave voltammetry (SWV). Detection of gaseous H_2O_2 is important in various fields, as in medicine, where gaseous H_2O_2 in the human breath is associated with a range of pathological conditions,²¹ as well as in the environment protection related to occupational risk of numerous hydrogen peroxide-related industries.²³ More importantly, gaseous H_2O_2 detection is a highly relevant subject for security issues, as most the homemade peroxo-explosives, which are frequently

misused in terroristic attacks (e.g., triacetone triperoxide or diacetone diperoxide) can be detected through gaseous H₂O₂.²⁴

On the other hand, the electrochemistry of copper species was exploited for the preparation of a variety of electrochemical sensors,²⁵ where copper was used either as an electrocatalyst (mostly in a form of copper nanoparticles),^{26,27} or using copper ions as a redox mediator.²⁸ As is well-known, electrochemical reduction of Cu²⁺ ions in a non-complexing aqueous medium follows a two-step mechanism (eqs. 1 and 3), proceeding via the formation of Cu⁺ ions as a labile intermediate, followed by a fast disproportionation reaction (2).^{29,30}



According to the Bockris-Mattson EE mechanism, the formal rate constant and potential of electrode reaction (3) are higher (in absolute values) in comparison to reaction (1).³¹ Thus, a typical cyclic voltammogram features a single pair of peaks, encompassing reactions (1-3). Apart from voltammetry, reactions (1-3) were also investigated and confirmed with microscopic techniques.^{32,33} In a complexing medium, an additional voltammetric response emerges due to reaction (4), where L is a complexing ligand.³⁴



The formal potential of reaction (4) is usually more negative than reactions (1) and (3). It is important to note that a particular reaction mechanism is highly sensitive to the experimental conditions (pH, concentration, and composition of the aqueous electrolyte, type of the working electrode, etc.) and can be significantly more complex than outlined above.^{35,36}

2. Experimental Section

All chemicals used were of analytical grade purity (Sigma-Aldrich). Aqueous solutions were prepared with purified water obtained from an Arium® mini-Plus purification system from Sartorius. PAA was in a non-cross-linked form with a molar mass of 450,000 g/mol. The stock solution of PAA was prepared by dissolving 0.1 g in 10 mL of distilled water. Stock solutions of 0.03 mol L⁻¹ copper(II) sulfate, 0.5 mol L⁻¹ potassium nitrate, and 0.1 mol L⁻¹ hydrogen peroxide were prepared in water. Accordingly, 1% (mass percent) of PAA solution at pH = 2.9, containing 0.1 mol L⁻¹ potassium nitrate, was the supporting electrolyte for the electrochemical study. Additionally, the concentration of copper(II) sulfate in the supporting electrolyte was 3×10^{-4} mol L⁻¹. In the conventional experiments where H₂O₂ was added to the supporting electrolyte, the concentration of H₂O₂ varied from 5×10^{-3} mol L⁻¹ to 1.5×10^{-2} mol L⁻¹. Experiments for studying the electrode mechanism were made with a glassy carbon as a working electrode, Ag/AgCl (3 mol L⁻¹ KCl) as a reference, and a carbon bar as a counter electrode. The electrolytic bridge connecting the reference electrode and the supporting electrolyte solution consisted of a 0.5 mol L⁻¹ KNO₃ aqueous solution to avoid leaking of Cl⁻ and formation of copper complexes. The glassy carbon electrode was cleaned with Al₂O₃ slurry, rinsed with water, and dried in the air prior to each experiment. All experiments were performed at room temperature, in air, and thus in the presence of dissolved oxygen, anticipating the analytical utility of the system for ambient gaseous H₂O₂ detection in the future.

Experiments for gaseous H₂O₂ detection were performed in a closed plastic chamber with a volume of 5 L using screen-printed carbon electrode (SPE) strips (Metrohm DropSens, 110) consisting of carbon as a working and counter electrode and Ag as a quasi-reference electrode. The aqueous solution of H₂O₂ with a volume of 50 mL and concentrations from 1×10^{-4} mol L⁻¹ to 1×10^{-2} mol L⁻¹ was placed in the closed plastic chamber for a few hours before electrochemical measurements to establish equilibrium between the liquid and gas phases. Fifty microliters (50 µL) of the supporting electrolyte containing 3×10^{-4} mol L⁻¹ copper(II) sulfate were drop-casted on the SPE strip covering all three electrodes. Afterwards, the modified SPE was inserted into the chamber and electrochemical measurements were performed after 1 min. Equilibration with the gaseous phase.

All electrochemical measurements were performed with an electrochemical measuring station µAutolab (potentiostat/galvanostat), model III, controlled by GPES software.

3. Results and Discussion

3.1. Studying the Basic Features of the Electrode Mechanism

The supporting electrolyte consisting of 1% (mass percent) PAA and potassium nitrate has a pH close to 3, which indicates that only a fraction of carboxylic groups of PAA are dissociated. Literature data indicate that Cu^{2+} ions are mainly in a hydrated form and less than 10% of dissolved Cu^{2+} ions are in a form of carboxylic complexes.³⁷ Thus, a typical voltammogram of Cu^{2+} ions in the studied supporting electrolyte at a glassy carbon electrode consists of a pair of voltametric peaks, in accord with the electrode mechanism described with eqs. (1–3) (Figure 1).

Figure 1. Typical cyclic staircase voltammogram of $3 \times 10^{-4} \text{ mol L}^{-1}$ Cu^{2+} ions (blue curve) in the supporting electrolyte containing 1% PAA and 0.1 mol L^{-1} KNO_3 with the step potential of $\Delta E = 1 \text{ mV}$ and the scan rate of $v = 10 \text{ mV/s}$ at a glassy carbon electrode. The red curve corresponds to the response of the supporting electrolyte in the absence of copper.

The broad, single cathodic peak reflects the electrode reductions of both Cu^{2+} and Cu^{1+} ions, affected by the chemical reaction (2), whereas the anodic peak represents the anodic stripping of the metallic copper deposited on the GC electrode surface. As the surface area of the anodic peak is smaller compared to the cathodic peak, it is possible that some of the reduced metallic copper are not deposited on the GC electrode surface, thus cannot be stripped from the electrode. Under corresponding experimental conditions, but in the absence of PAA, the cyclic voltammogram differs in the morphology of the anodic stripping peak. Specifically, it is significantly broader compared to PAA, while the anodic peak-current and peak-potential are virtually identical in both cases (data not shown). Thus, large polymeric molecules of PAA affect the morphology of the metal copper deposit, most likely causing the formation of a uniform metallic film. The morphology and the peak current of the cathodic peak are also different (peak current is smaller with PAA); however, the cathodic peak potentials are comparable in both cases (data not shown).

As can be seen from Figure 1 (blue curve), the copper deposition gives rise to enhancement of the cathodic tail of the voltammogram at potentials more negative than -0.400 V, implying an electrocatalytic effect toward the reduction of dissolved oxygen and/or hydrogen ions. It is important to note that an additional irreproducible reduction peak of a small intensity emerges at potentials around -0.325 V, which might be associated with the reaction described with eq (4), where PAA is the complexing ligand. The latter reduction peak is most frequently covered with the baseline current.

Consecutive potential cycling shows that, after six cycles, a stable voltammogram is obtained, noting that the differences between the third and the sixth cycles are minor (Figure 2).

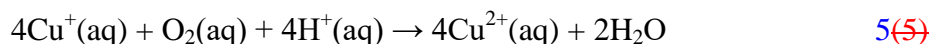
Figure 2. Consecutive cycles in cyclic staircase voltammetry, showing 1st, 2nd, 3rd and 6th voltammograms. The direction of arrows indicates the change of the response by increasing the serial number of the potential cycle. Other conditions are identical as in Figure 1.

Moreover, cleaning the GC electrode and repeating the voltammetric experiment results in a reproducible response, implying that the film growth stabilizes after several potential cycles and can be completely removed from the electrode surface by mechanical cleaning. The relative simplicity and reproducibility of the voltammetric response under studied conditions indicate that no other copper oxides/hydroxides are formed, which is in accord with the theoretical Pourbaix diagrams of copper.³⁸

Further insights into the mechanistic aspects of the reduction mechanism have been obtained by inspecting the role of the vertex potential (E_v) at the side of negative potentials. The cyclic voltammetric response recorded from 0.300 V and a vertex potential more positive than -0.150 V consists of a cathodic peak only (Figure 3).

Figure 3. Typical cyclic staircase voltammograms for Cu^{2+} reduction recorded from the starting potential of 0.300 V by shifting the vertex potential (E_v) from $E_v = -0.050$ V (red), -0.100 V (blue), -0.15 V (green), and -0.500 V (inset, violet curve). Other conditions are identical as in Figure 1.

For $E_v = -0.150$ V (green curve in Figure 3), a very small anodic peak emerges, which progressively enlarges by shifting the vertex potential toward more negative values, eventually evolving to a strong anodic stripping peak for $E_v = -0.500$ V (the inset of Figure 3, which represents the typical voltammetric response, shown also in Figures 1 and 2). Obviously, the elemental copper deposit on the GC electrode surface is not formed in a sufficient amount when the cyclic voltammetry is conducted at the scan rate of 10 mV/s with a vertex potential equal to or more positive than -0.150 V. Under these conditions, the lack of any oxidation peak in cyclic voltammograms implies that Cu^+ ions, as an intermediate species, are not stable and disproportionate according to reaction (2). Interestingly, in spite of the fact that one of the products of disproportionation reaction (2) is elemental copper, it cannot be electrochemically oxidized. This finding is in accordance with the previous finding that the surface area of the anodic peak is smaller compared to the cathodic peak (Figure 1). The most probable reason is that the elemental copper formed by homogeneous chemical reaction (2) is in a form of colloidal copper particles stabilized by PAA,³⁹ rather than being in a form of a metal deposit on the electrode surface. Thus, the copper deposit on the electrode surface is mainly formed by the electrode reaction (3). It should be noted that, besides reaction (2), the electrochemically formed Cu^+ ions can be oxidized back to Cu^{2+} by dissolved oxygen (eq. 5):



Yet, according to the literature data, reaction (5) is significantly slower than reaction (2).⁴⁰

Further analysis of the critical potential and time required for producing copper deposit on the electrode surface according to electrode reaction (3) has been done by cyclic voltammetry starting at negative potentials. As illustrated in Figure 4, the intensity of the anodic stripping peak depends on both initial potential and deposition time.

Figure 4. Cyclic staircase voltammograms recorded at the initial potential of -0.15 V (red curve) and -0.1 V (blue curve) with electrochemical deposition, at the initial potential, of 60 s. Dotted lines represent voltammograms without deposition. Other conditions are identical as in Figure 1.

For instance, a deposition process of 60_s at the potential of -0.150 _V results in a sufficient amount of copper deposit, thus enabling an anodic stripping peak to evolve (Figure 4, red curve). Moreover, the blue voltammogram in Figure 4, recorded by deposition at -0.100 _V, is characterized with a small anodic stripping peak. Rigorously speaking, a small anodic stripping peak emerges even at deposition potentials more positive than -0.100 _V if the deposition time is sufficiently long. Thus, one can speculate that the formal potential of reaction (3) is more positive than reaction (1), which is in accord with the literature data.³¹

The complexity of this two-step electron transfer mechanism arises additionally from the fact that the intermediary species Cu^+ are competitively consumed by the homogeneous redox reactions (2) and the electrode reaction (3) (while the rate of reaction (5) is assumed to be insignificant compared to reaction (2)⁴⁰). Cyclic voltammetry conducted at scan rates up to 200_mV/s, within the potential window from 0.300_V to -0.150 _V (data not shown), does not result in an anodic peak due to electrochemical reoxidation of Cu^+ to Cu^{2+} , which indicates that the rate of reaction (2) is relatively high. Using however SWV, as a significantly faster technique, an anodic peak emerges by increasing the frequency of potential modulation (Figure 5).

Figure 5. Typical square-wave voltammograms for the reduction of Cu^{2+} ions recorded with the frequency values of 1_Hz (A), 5_Hz (B), 10_Hz (C), and 50_Hz (D) showing forward (reduction, red curve), backward (oxidation, blue curve), and net (green curve) components at the starting potential $E_{\text{start}} = -0.6$ _V, SW amplitude $E_{\text{sw}} = -50$ _mV, and the step potential $E_{\text{step}} = -1$ _mV. Other conditions are identical as in Figure 1.

The backward, anodic component of the SW voltammetric response has a diffusion-affected character, rather than being an anodic stripping peak. Its intensity enlarges relative to the forward (reductive) component in proportion to the frequency. Hence, it corresponds to the electrochemical oxidation of Cu^+ back to Cu^{2+} ions, circumventing the effect of the chemical reaction (2). In order to get an impression of the critical time window of the SW voltammetric experiment, let us note that the duration of a single SW potential pulse, for instance at 50_Hz, is

only 10 ms.⁴¹ In the course of two adjacent pulses (i.e., within the time interval of 20 ms), the reduction of Cu^{2+} and reoxidation of electrochemically formed Cu^{1+} ions take place, thus rendering homogenous chemical reaction (2) less effective. The appearance of an anodic peak in the SW voltammograms at higher frequencies also implies that Cu^{+} ions are not instantly transformed electrochemically to Cu(s) according to reaction (3), indicating a degree of stabilization~~stabilisation~~ within the polymer molecules of PAA.

Addition of H_2O_2 to the experimental system increases the reduction peak in CSV, most probably as a consequence of an EC' reaction pathway (Figure 6).⁴²⁻⁴⁴

Figure 6. ~~The e~~Effect of the increasing concentration of H_2O_2 on the cyclic staircase voltammetric response of Cu^{2+} ions. The red voltammogram shows the response of Cu^{2+} without H_2O_2 . The arrows indicate the variation of the response by adding H_2O_2 at ~~a~~concentrations of 5×10^{-3} , 1×10^{-2} , and $1.5 \times 10^{-2} \text{ mol L}^{-1}$. Other conditions are identical as in Figure 1.

-In the presence of H_2O_2 , the reduction current starts increasing even at positive potentials of 0.050 V (cf. Figure 6), transforming the cathodic peak into a sigmoid curve. Hence, it is plausible to assume that the redox couple $\text{Cu}^{2+}/\text{Cu}^{+}$ acts as a redox mediator for the indirect electrochemical reduction of H_2O_2 . Moreover, at potentials more negative than -0.300 V , a strong increase of the reduction current tail occurs, associated with direct H_2O_2 reduction on the copper-modified GC electrode. Interestingly, the reduction tail does not form a voltammetric peak at more negative potentials (data not shown) indicating that the electrode process is not limited by the diffusional mass transfer of hydrogen peroxide. Most likely a complex radical-type electrode mechanism takes place initiated by the reduction of H_2O_2 on the metallic copper particles, involving further the aqueous phase in the overall electrode mechanism.^{44,45}

Mechanistic considerations at GCE are expected to be similar at screen-printed carbon electrodes, anticipating a plausible difference in the kinetics of both electrode reactions (1) and (3). Figure 7 compares typical SW voltammograms for the reduction of Cu^{2+} ions at two electrodes.

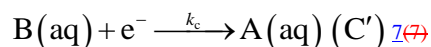
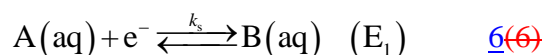
Figure 7. Typical SW voltammograms for the reduction of Cu^{2+} at glassy carbon (A) and [the](#) screen-printed carbon electrode (B), showing forward (red), backward (blue), and net (green) voltammetric components. SW frequency is 10 Hz, and other potential modulation parameters are identical as in Figure 5. The silver wire serves as a pseudo reference electrode in (B). Other conditions are identical as in Figure 1.

Evidently, the absolute current and potential values are not directly comparable owing to the discrepancies between the working electrode surface area and ~~the~~ reference electrodes (i.e., Ag/AgCl (3 mol L⁻¹ KCl) and a silver wire for GCE and SPE, respectively). Yet, a comparison of the relative parameters, such as the ratio of the peak currents of the forward and backward SW voltammetric components ($I_{p,f}/I_{p,b}$), is highly indicative of mechanistic considerations. Specifically, the ratio is $I_{p,f}/I_{p,b} = 10$ and 1.5 for GCE and SPE, respectively. The anodic, backward voltammetric component assigned to the electrochemical reoxidation Cu^+ to Cu^{2+} is significantly more developed at SPE (cf. Figure 7). Apparently, the stability of Cu^+ in the vicinity of the electrode is more pronounced at SPE than at GCE. Considering that the composition of the medium is identical for both electrodes, the only reason for such obvious differences arises from the slower electrode kinetics of the second electrode reaction (3), which competitively exhausts Cu^+ ions in parallel with the reaction (2). The last conclusion is in [favor](#) of the analytical detection of H_2O_2 on an SPE via an EC' mechanism where the $\text{Cu}^{2+}/\text{Cu}^+$ couple serves as a redox mediator.

3.2. Theoretical [C](#)onsideration and [S](#)imulations of the [E](#)lectrode [M](#)echanism

~~In order to~~ To provide further insights into the complex voltammetric features of the studied electrode mechanism, the voltammetric outcome was briefly [analyzed](#) using numerical simulations. In a first approximation, an $\text{E}_1\text{C}'\text{E}_2$ reaction mechanism has been assumed at a planar electrode of dissolved species, considering semi-infinite diffusional mass

transport (eqs. ~~6~~–~~8~~). The first electron transfer step E_1 (eq. ~~6~~), corresponding to the reduction of Cu^{2+} to Cu^+ (eq. ~~1~~), is assumed to be electrochemically quasireversible,⁴³ whereas the second electrode reaction E_2 (eq. ~~8~~), which corresponds to the reduction of Cu^+ to $\text{Cu}(0)$ (eq. ~~3~~), is simulated as being electrochemically reversible. To tackle the mathematical complexity of the experimental system, the disproportionation reaction of Cu^+ ions (eq. ~~3~~) is assimilated as being a simple, regenerative reaction C' (eq. ~~7~~).⁴⁶



Details on the mathematical ~~modelling~~ modelling by means of the step-function method are given elsewhere.⁴¹

Initial simulations have been focused on understanding the morphology and evolution of the cathodic peak under conditions of cyclic staircase voltammetry (cf. Figures ~~1~~–~~4~~). Critical parameters controlling the voltammetric response are the electrode kinetic parameter of the first electrode reaction ~~κ~~ κ , the potential difference between the formal reduction potentials of the first and the second electrode reaction, ~~$\Delta E = E^{\theta}_1 - E^{\theta}_2$~~ $\Delta E = E^{\theta}_1 - E^{\theta}_2$, and the rate constant k_c (s^{-1}) of the regenerative chemical reaction C' (eq. ~~7~~). The electrode kinetic parameter controlling the electrochemical reversibility of the first electrode reaction is defined as $\kappa = k_s \sqrt{\frac{\tau}{D}}$, where k_s is the standard rate constant ($\text{cm} \cdot \text{s}^{-1}$), ~~τ~~ τ is the duration of a single potential tread in staircase voltammetry, and D is the common diffusion coefficient. All three parameters, ~~κ~~ κ , ~~ΔE~~ ΔE , and k_c have been systematically studied, over a broad range of values. Specifically, the first electrode reaction was assumed to be typically quasireversible characterized by the electrode kinetic parameter within the interval ~~$-0.42 \leq \log(\kappa) \leq 0.40$~~ $-0.42 \leq \log(\kappa) \leq 0.40$; the potential difference was varied from ~~$\Delta E = 0.200$~~ $\Delta E = 0.200$ V (meaning that the formal reduction potential of the second electrode reaction is more negative than the first one) to ~~$\Delta E = -0.300$~~ $\Delta E = -0.300$ V typical for ~~an~~ $E_1 E_2$

mechanism with inverted potentials,⁴⁷ as expected for the copper system, and the catalytic rate constant was altered over the interval $\log(k_c/s^{-1}) \leq 11$.

Under conditions of cyclic staircase voltammetry, when the simulation was conducted at a relatively slow scan rate of $v = 10$ mV/s (corresponding to the conditions of Figure 1), the morphology of the cathodic peak depends predominantly on the value of ΔE and k_c , as shown in Figure 8A.

Figure 8. (A) Comparison of the experimental (blue line) with theoretical voltammograms considering the cathodic peak of the cyclic staircase voltammetry. Simulation conditions are: $T = 298.15$ K, electron transfer coefficient $\alpha = 0.5$, and step potential $dE = 1$ mV. The other conditions specific for each theoretical voltammogram are: $k_c = 1$, $\Delta E = -0.2$ V, and $k_c = 10^5$ s⁻¹ (red line); $k_c = 0.398$, $\Delta E = 0$ V, and $k_c = 10^5$ s⁻¹ (green line); and $k_c = 0.398$, $\Delta E = -0.2$ V, and $k_c = 10^7$ s⁻¹ (black line). (B) The best fit between experimental (blue line) and theoretical (red line) found for $k_c = 0.398$, $\Delta E = -0.2$ V, and $k_c < 10^5$ s⁻¹. The inset shows the linearity of the best fit in potential interval from 0.15 V to 0.168 V. Experimental conditions are identical as in Figure 1.

The best fit is achieved by assuming a mechanism with inverted formal reduction potentials, i.e., $\Delta E = -0.200$ V and the electrode kinetic parameter of $k_c = 0.398$ (Figure 8B). Under these conditions, the intensity of the response is virtually identical regardless of the kinetics of the chemical reaction over the interval $k_c < 10^5$ s⁻¹, implying that the rate of the chemical reaction cannot be unambiguously estimated and the voltammetric features are predominantly controlled by the inverted potential difference of $\Delta E = -0.200$ V. Let us note that, in a pure aqueous medium, the potential difference between reactions (1) and (3) is $\Delta E = -0.361$ V. Thus, Cu⁺ ions are significantly stabilized in the presence of PAA.

Fitting the dimensionless theoretical current function defined as $\psi = I/A$, with the experimental current (I), the value of the amperometric constant $A = 2.35 \times 10^{-5}$ A was found by the simulations. Let us note that the amperometric constant is defined as $A = nFSc^*(D/\tau)^{1/2}$, where n is the number of electrons in a single electron transfer step, F is the Faraday constant, S

is the electrode surface area, and c^* is the bulk concentration of the initial reactant. Knowing that $n = 1$, $S = 7.1 \times 10^{-2} \text{ cm}^2$, $c^* = 3 \times 10^{-4} \text{ mol dm}^{-3}$, and $\tau = 0.1 \text{ s}$, the diffusion coefficient estimated from the value of the amperometric constant is $D = 1.3 \times 10^{-5} \text{ cm}^2/\text{s}$, which is in excellent agreement with the literature data.³⁰ Thus, from the definition of the electrode kinetic parameter $\kappa = k_s \sqrt{\frac{\tau}{D}}$, and value of $\kappa = 0.398$ found by fitting procedure, the estimated value of the standard rate constant is $k_s = 4.5 \times 10^{-3} \text{ cm s}^{-1}$. The inset of Figure 8B shows the simple correlation between theoretical and experimental data in the potential interval from 0.150 V to -0.168 V, represented by a linear regression line ($R^2 = 0.999$) with a slope close to 1 and an intercept close to zero, inferring high reliability of the estimated parameters.

Further simulations have been conducted by SWV, attempting to get an impression of the value of the chemical rate constant k_c (rigorously speaking, it is an apparent rate constant, as the real disproportionation reaction (eq. 2) is approximated as a first-order regenerative chemical reaction (eq. 7)). The value of k_c has been systematically altered over the interval $0 \leq \log(k_c/\text{s}^{-1}) \leq 5$, for three SW frequencies of 5, 10, and 50 Hz. The other parameters have been set to the values estimated in previous simulations (i.e., $k_s = 4.5 \times 10^{-3} \text{ cm s}^{-1}$, $D = 1.3 \times 10^{-5} \text{ cm}^2/\text{s}$, and $\Delta E = -0.200 \text{ V}$). Comparing the morphological evolution of the forward and backward SW voltammetric components with the frequency, it has been established that the experimental voltammograms presented in Figure 5 can be reproduced assuming a value of the chemical rate constant to fall within the interval $2 \leq \log(k_c/\text{s}^{-1}) \leq 3$. To the best of our knowledge, kinetic information on the disproportionation reaction in an aqueous medium was not reported so far. The main reason is that the reaction is extremely fast, and only the equilibrium constant in the order of 10^6 was estimated.⁴⁸ In the present system, although the rate constant is roughly estimated, the value suggests certain stabilization of Cu^+ by PAA.

3.3. Analytical Application

Physicochemical properties of PAA, i.e., its ability to absorb gases, and small volume of the hydrogel on screen-printed electrodes should enable a high concentration of H_2O_2 and at the

same time offer high chemical stability in the gel phase and fast equilibration of H₂O₂ on the gas/liquid interface. For this reason, SPE was modified with a 50- μ L aqueous solution of PAA, containing KNO₃ and Cu²⁺ ions. The modified SPE was inserted in the chamber containing gaseous H₂O₂, with a previously established equilibrium between the liquid and the gas phases. Electrochemical measurements were performed after 1-min. equilibration with the gaseous phase.

Concentration analysis has been done over the interval from 0.1 mmol/L to 10 mmol/L, taking into account the concentration of the aqueous solution of H₂O₂ inserted in the gas chamber. The corresponding concentration interval for the gaseous H₂O₂ is 7.27×10^{-8} – 7.27×10^{-6} mmol/L, estimated utilizing Henry's law.^{49,50} Calibration curves were constructed and compared for cyclic staircase voltammetry, chronoamperometry, and square-wave voltammetry (Figure 9).

Figure 9. Calibration curves constructed for different concentrations of aqueous solutions of H₂O₂ in the chamber using SPE at $T = 303$ K. Electrochemical signal was measured after a 1-min. equilibration period of the modified SPE in the chamber using cyclic staircase voltammetry (a), chronoamperometry (b), and SW voltammetry (c, right ordinate). For CSV: $v = 50$ mV/s; $E_{\text{step}} = 5$ mV; $E_1 = 0.3$ V (third potential scan used for calibration line). For SWV: $E_{\text{sw}} = 50$ mV; $f = 10$ Hz; $E_{\text{step}} = 1$ mV; $E_1 = 0.3$ V. For CA: $E = -0.4$ V, $t = 10$ s. For all techniques: SPCE—working electrode; Ag—reference electrode. Other conditions are identical as in Figure 1.

For the calibration line constructed by CSV, the reduction peak-current was measured by applying a tangent to estimate the background current (Figure 9, curve a). In SWV, the absolute peak current values of the net component were measured. The concentration dependence under conditions of SWV (Figure 9, curve c) is more complex. The dependence can be linearized over two separate concentration intervals, i.e., from 0 mmol/L to 1 mmol/L ($R^2 = 0.9545$) and from 1 mmol/L to 10 mmol/L ($R^2 = 0.9946$). The complexity of the concentration analysis with SWV clearly reflects the underlying complexity of the electrode mechanism, most likely due to the competition of the redox reactions of H₂O₂ with Cu⁺ ions and the disproportionation reaction (2).

The calibration line constructed by CA is based on current values measured at a potential of -0.400 V (vs. Ag-pseudo-reference electrode, cf. Figure 7B) after 10 s. The limit of detection (LOD) and the limit of quantification (LOQ) were calculated for gaseous H_2O_2 according to $\text{LOD} = 3S_a/b$ and $\text{LOQ} = 10S_a/b$, where S_a is the standard deviation of the response of the linear regression and b is the slope of the calibration line (Table 1).

Table 1. Limit of Detection (LOD) and Limit of Quantification (LOQ) for gaseous H_2O_2 measured with CSV, SWV, and CA on an SPE. ~~Other conditions are identical as in Figure 9.~~

Technique	LOD (gaseous H_2O_2)/ $\mu\text{g dm}^{-3}$	LOQ (gaseous H_2O_2)/ $\mu\text{g dm}^{-3}$
CV	$3.49 \cdot 10^{-2}$	$1.16 \cdot 10^{-1}$
CA	$4.58 \cdot 10^{-2}$	$1.51 \cdot 10^{-1}$
SWV	$1.44 \cdot 10^{-1}$	$4.75 \cdot 10^{-1}$

~~Other conditions are identical as in Figure 9.~~

Although the overall reaction pathway of Cu^{2+} reduction in the presence of hydrogen peroxide does not depend on the electrochemical technique applied, the differences in potential modulation and the critical time of the electrochemical experiment, cause different aspects of the complex mechanism to prevail under given conditions; thus, differences in the analytical outcome are likely. For instance, the critical time window is in the millisecond range for the experiment under conditions of SWV, while it is in a second range for CSV and CA experiments, which is critically important for the overall effect of both redox reactions of H_2O_2 and disproportionation of Cu^+ .

4. Conclusions

To the best of our knowledge, it is the first mechanistic analysis of copper(II) reduction in PAA aqueous solution using voltammetric techniques. Experimental data, together with the theoretical considerations and simulations of the voltammetric response, confirm that the reaction pathway is similar to in a pure aqueous medium, with indications that the intermediate Cu^+ ions are partly stabilized by PAA, and their further reduction is thermodynamically less favored, while the kinetics of their disproportionation is diminished in comparison to a pure aqueous medium.

Moreover, at commercially available carbon SPE, the reduction of Cu^+ to the elemental copper is electrochemically slower than at GCE, which is beneficial for analytical purposes for H_2O_2 detection where the $\text{Cu}^{2+}/\text{Cu}^+$ couple serves as a redox mediator. SPE covered with a thin film of 50- μL aqueous solution of PAA, containing KNO_3 and Cu^{2+} ions, is evidently a promising platform for detection of gaseous H_2O_2 in the presence of oxygen with a superior limit of detection ranging in the sub- $\mu\text{g}\cdot\text{dm}^{-3}$ concentration level.

Acknowledgements

The authors would ~~would~~ like to acknowledge with gratitude the support from the National Science Centre of Poland through the Opus Lap grant no. 2020/39/I/ST4/01854.

References

1. Abdelaal, M. Y.; Makki, M. S. I.; Sobahi, T. R. A. Modification and characterization of polyacrylic acid for metal ion recovery. *Am. J. Polym. Sci. American Journal of Polymer Science*. **2012**, *2*, 73–78, [10.5923/j.ajps.20120204.05](https://doi.org/10.5923/j.ajps.20120204.05).
2. Nho, Y.-C.; Park, J.-S.; Lim, Y.-M. Preparation of poly(acrylic acid) hydrogel by radiation crosslinking and its application for mucoadhesives. *PolymerPolymers* **2014**, *6*, 890–898, [10.3390/polym6030890](https://doi.org/10.3390/polym6030890).
3. Yin, M. J.; Yao, M.; Gao, S.; Zhang, A. P.; Tam, H. Y.; Wai, P. K. A. Rapid 3D patterning of poly (acrylic acid) ionic hydrogel for miniature pH sensors. *Adv. Mater. Advanced Materials* **2016**, *28* (7), 1394–1399, [10.1002/adma.201504021](https://doi.org/10.1002/adma.201504021).
4. Bastakoti, B. P.; Guragain, S.; Nakashima, K.; Yamauchi, Y. Stimuli-induced core–corona inversion of micelle of poly(acrylic acid)-block-poly(N-isopropylacrylamide) and its application in drug delivery. *Macromol. Chem. Phys.* **2015**, *216*, 287–291, [10.1002/macp.201400440](https://doi.org/10.1002/macp.201400440).
5. Braam, K.; Subramanian, V. Astencil printed, high energy density silver oxide battery using a novel photopolymerizable poly(acrylic acid) separator. *Adv. Mater.* **2015**, *27*, 689–694, [10.1002/adma.201404149](https://doi.org/10.1002/adma.201404149).
6. Zhao, Q.; Yin, M.; Zhang, A. P.; Prescher, S.; Antonietti, M.; Yuan, J. Hierarchically structured nanoporous poly (ionic liquid) membranes: Facile preparation and

- application in fiber-optic pH sensing. *J. Am. Chem. Soc. Journal of the American Chemical Society* **2013**, 135 (15), 5549–5552, [10.1021/ja402100r](https://doi.org/10.1021/ja402100r).
7. Zhao, Q.; Dunlop, J. W. C.; Qiu, X.; Huang, F.; Zhang, Z.; Heyda, J.; Dzubiella, J.; Antonietti, M.; Yuan, J. An instant multi-responsive porous polymer actuator driven by solvent molecule sorption. *Nat. Commun. Nature communications* **2014**, **5** (1), 1–8, [10.1038/ncomms5293](https://doi.org/10.1038/ncomms5293).
 8. Zhao, C.; Nie, S.; Tang, M.; Sun, S. Polymeric pH-sensitive membranes—A review. *Prog. Polym. Sci. Progress in Polymer Science* **2011**, 36 (11), 1499–1520, [10.1016/j.progpolymsci.2011.05.004](https://doi.org/10.1016/j.progpolymsci.2011.05.004).
 9. Yin, M. J.; Wu, C.; Shao, L. Y.; Chan, W. K. E.; Zhang, A. P.; Lu, C.; Tam, H. Y. Label-free, disposable fiber-optic biosensors for DNA hybridization detection. *Analyst* **2013**, 138 (7), 1988–1994, [10.1039/c3an36791f](https://doi.org/10.1039/c3an36791f).
 10. Gu, B.; Yin, M. J.; Zhang, A. P.; Qian, J. W.; He, S. Fiber-optic metal ion sensor based on thin-core fiber modal interferometer with nanocoating self-assembled via hydrogen bonding. *Sens. Actuators, B Sensors and Actuators B: Chemical* **2011**, 160 (1), 1174–1179, [10.1016/j.snb.2011.09.043](https://doi.org/10.1016/j.snb.2011.09.043).
 11. Pearson, A. C.; Linford, M. R.; Harb, J. N.; Davis, R. C. Dual patterning of a poly (acrylic acid) layer by electron-beam and block copolymer lithographies. *Langmuir* **2013**, 29 (24), 7433–7438, [10.1021/la304486x](https://doi.org/10.1021/la304486x).
 12. Chiang, E. N.; Dong, R.; Ober, C. K.; Baird, B. A. Cellular responses to patterned poly (acrylic acid) brushes. *Langmuir* **2011**, 27 (11), 7016–7023, [10.1021/la200093e](https://doi.org/10.1021/la200093e).
 13. Hwang, I. T.; Oh, M. S.; Jung, C. H.; Choi, J. H. Direct patterning of poly (acrylic acid) on polymer surfaces by ion beam lithography for the controlled adhesion of mammalian cells. *Biotechnol. Lett. Biotechnology letters* **2014**, 36 (10), 2135–2142, [10.1007/s10529-014-1569-3](https://doi.org/10.1007/s10529-014-1569-3).
 14. Wang, Y. M.; Cui, Y.; Cheng, Z. Q.; Song, L. S.; Wang, Z. Y.; Han, B. H.; Zhu, J. S. Poly (acrylic acid) brushes pattern as a 3D functional biosensor surface for microchips. *Appl. Surf. Sci. Applied surface science* **2013**, 266, 313–318, [10.1016/j.apsusc.2012.12.017](https://doi.org/10.1016/j.apsusc.2012.12.017).
 15. Mandel, M. The potentiometric titration of weak polyacids. *Eur. Polym. J. European Polymer Journal* **1970**, 6 (6), 807–822, [10.1016/0014-3057\(70\)90005-4](https://doi.org/10.1016/0014-3057(70)90005-4).
 16. Terao K. Poly(acrylic acid) (PAA). In: Kobayashi S.; Müllen K.; (Eds.); *Encyclopedia of Polymeric Nanomaterials*; Springer; Berlin, Heidelberg, 2014, [10.1007/978-3-642-36199-9_279-1](https://doi.org/10.1007/978-3-642-36199-9_279-1).

17. Swift, T.; Swanson, L.; Geoghegan, M.; Rimmer, S. The pH-responsive behaviour of poly (acrylic acid) in aqueous solution is dependent on molar mass. *Soft Matter* **2016**, *12* (9), 2542–2549, [10.1039/C5SM02693H](https://doi.org/10.1039/C5SM02693H).
18. Isailović, J.; Vidović, K.; Hočevan, S. B. Simple electrochemical sensors for highly sensitive detection of gaseous hydrogen peroxide using polyacrylic-acid-based sensing membrane. *Sens. Actuators, B: Chemical* **2022**, *352*, 131053, [10.1016/j.snb.2021.131053](https://doi.org/10.1016/j.snb.2021.131053).
19. Wang, Z.; Wang, Z.; Zhang, H.; Duan, X.; Xu, J.; Wen, Y. Electrochemical sensing application of poly (acrylic acid modified EDOT-co-EDOT): PSS and its inorganic nanocomposite with high soaking stability, adhesion ability and flexibility. *RSC Adv.* **2015**, *5* (16), 12237–12247, [10.1039/C4RA10970H](https://doi.org/10.1039/C4RA10970H).
20. Ricardo Teixeira Tarley, C.; de Cássia Mendonça, J.; Rianne da Rocha, L.; Boareto Capelari, T.; Carolyne Prete, M.; Cecílio Fonseca, M.; Midori de Oliveira, M.; César Pereira, A.; Luiz Scheel, G.; Bastos Borges, K.; Gava Segatelli, M. Development of a molecularly imprinted poly (acrylic acid)-mwcnt nanocomposite electrochemical sensor for tramadol determination in pharmaceutical samples. *Electroanalysis* **2020**, *32* (5), 1130–1137, [10.1002/elan.201900148](https://doi.org/10.1002/elan.201900148).
21. Loukides, S.; Horvath, I.; Wodehouse, T.; Cole, P. J.; Barnes, P. J. Elevated levels of expired breath hydrogen peroxide in bronchiectasis. *Am. J. Respir. Crit. Care Med.* **1998**, *158* (3), 991–994, [10.1164/ajrccm.158.3.9710031](https://doi.org/10.1164/ajrccm.158.3.9710031).
22. Sznajder, J. I.; Fraiman, A.; Hall, J. B.; Sanders, W.; Schmidt, G.; Crawford, G.; Nahum, A.; Factor, P.; Wood, L. D. H. Increased hydrogen peroxide in the expired breath of patients with acute hypoxemic respiratory failure. *Chest* **1989**, *96* (3), 606–612, [10.1378/chest.96.3.606](https://doi.org/10.1378/chest.96.3.606).
23. Mucci, N.; Dugheri, S.; Bonari, A.; Farioli, A.; Rapisarda, V.; Garzaro, G.; Cappelli, G.; Arcangeli, G. Health risk assessment related to hydrogen peroxide presence in the workplace atmosphere-analytical methods evaluation for an innovative monitoring protocol. *Int. J. Occup. Med. Environ. Health* **2020**, *33* (2), 137–150, [10.13075/ijomeh.1896.01508](https://doi.org/10.13075/ijomeh.1896.01508).
24. Chen, Q.; Yang, L.; Guo, K.; Yang, J.; Han, J. M. Expedite Fluorescent Sensor Prototype for Hydrogen Peroxide Detection with Long-Life Test Substrates. *ACS Omega* **2021**, *6* (17), 11447–11457, [10.1021/acsomega.1c00471](https://doi.org/10.1021/acsomega.1c00471).

25. Zhu, H.; Zhang, S.; Li, M.; Shao, Y.; Zhu, Z. Electrochemical sensor for melamine based on its copper complex. *Chem. Commun. Chemical Communications* **2010**, 46 (13), 2259–2261, [10.1039/b924355k](https://doi.org/10.1039/b924355k).
26. Ye, W.; Guo, X.; Ma, T. A review on electrochemical synthesized copper-based catalysts for electrochemical reduction of CO₂ to C₂+ products. *Chem. Eng. J. Chemical Engineering Journal* **2021**, 414, 128825, [10.1016/j.cej.2021.128825](https://doi.org/10.1016/j.cej.2021.128825).
27. Welch, C. M.; Compton, R. G. The use of nanoparticles in electroanalysis: a review. *Anal. Bioanal. Chem. Analytical and bioanalytical chemistry* **2006**, 384 (3), 601–619, [10.1007/s00216-005-0230-3](https://doi.org/10.1007/s00216-005-0230-3).
28. Evans, J.; Pletcher, D.; Warburton, P. R. G.; Gibbs, T. K. A new electrochemical sensor for carbon dioxide: Part 2. Study of the sensor chemistry. *J. Electroanal. Chem. Interfacial Electrochem. Journal of electroanalytical chemistry and interfacial electrochemistry* **1989**, 262 (1–2), 119–129, [10.1016/0022-0728\(89\)80016-6](https://doi.org/10.1016/0022-0728(89)80016-6).
29. Altermatt, J. A.; Manahan, S. E. Electrochemical behavior of cuprous ion in a noncomplexing aqueous medium. *Anal. Chem. Analytical Chemistry* **1968**, 40 (3), 655–657, [10.1021/ac60259a030](https://doi.org/10.1021/ac60259a030).
30. Tindall, G. W.; Bruckenstein, S. Determination of heterogeneous equilibrium constants by chemical stripping at a ring-disk electrode. Evaluation of the equilibrium constant for the reaction copper+ copper(II)-> 2copper(I) in 0.2M sulfuric acid. *Analytical Anal. Chemistry Chem.* **1968**, 40 (10), 1402–1404, [10.1021/ac60266a017](https://doi.org/10.1021/ac60266a017).
31. Mattsson, E.; Bockris, J. O'M. Galvanostatic studies of the kinetics of deposition and dissolution in the copper+ copper sulphate system. *Trans. Faraday Soc. Transactions of the Faraday Society* **1959**, 55, 1586–1601, [10.1039/tf9595501586](https://doi.org/10.1039/tf9595501586).
32. Grujicic, D.; Pesic, B. Reaction and nucleation mechanisms of copper electrodeposition from ammoniacal solutions on vitreous carbon. *Electrochim. Acta Electrochimica Acta* **2005**, 50 (22), 4426–4443, [10.1016/j.electacta.2005.02.012](https://doi.org/10.1016/j.electacta.2005.02.012).
33. Grujicic, D.; Pesic, B. Electrodeposition of copper: the nucleation mechanisms. *Electrochim. Acta Electrochimica acta* **2002**, 47 (18), 2901–2912, [10.1016/S0013-4686\(02\)00161-5](https://doi.org/10.1016/S0013-4686(02)00161-5).
34. Bolzán, A. E. Electrodeposition of copper on glassy carbon electrodes in the presence of picolinic acid. *Electrochim. Acta Electrochimica Acta* **2013**, 113, 706–718, [10.1016/j.electacta.2013.09.132](https://doi.org/10.1016/j.electacta.2013.09.132).

35. Cheng, B.; Yi, H.; He, C.; Liu, C.; Lei, A. Revealing the ligand effect on copper-(I) disproportionation via operando IR spectra. *Organometallics* **2015**, *34* (1), 206–211, [10.1021/om501053k](https://doi.org/10.1021/om501053k).
36. Rosen, B. M.; Jiang, X.; Wilson, C. J.; Nguyen, N. H.; Monteiro, M. J.; Percec, V. The disproportionation of Cu-(I)-X mediated by ligand and solvent into Cu-(0) and Cu (II)-X₂ and its implications for SET-LRP. *J. Polym. Sci., Part A: Polym. Chem. Journal of Polymer Science Part A: Polymer Chemistry* **2009**, *47* (21), 5606–5628, [10.1002/pola.23690](https://doi.org/10.1002/pola.23690).
37. Chevtaev, A. S.; Tabunshchikov, A. I.; Ozerin, A. S.; Radchenko, F. S.; Novakov, I. A. Interaction of Polyacrylic Acid with Copper, Cobalt, and Nickel Ions in Aqueous Solutions. *Russ. J. Gen. Chem. Russian Journal of General Chemistry* **2020**, *90* (5), 870–873, [10.1134/S1070363220050187](https://doi.org/10.1134/S1070363220050187).
38. Takeno, N. Atlas of Eh-pH diagrams. *Geological Geol. Survey of Japan. Open-File Report* **2005**, *419*, 102.
39. Guo, H.; Chen, Y.; Cortie, M. B.; Liu, X.; Xie, Q.; Wang, X.; Peng, D. L. Shape-selective formation of monodisperse copper nanospheres and nanocubes via disproportionation reaction route and their optical properties. *The Journal of Physical Phys. Chemistry Chem. C* **2014**, *118* (18), 9801–9808, [10.1021/jp5014187](https://doi.org/10.1021/jp5014187).
40. Papassiopi, N.; Gaunand, A.; Renon, H. Oxidation of Cu-(I) by oxygen in concentrated NaCl solutions—I. Homogeneous kinetics of oxidation by molecular oxygen in solution. *Chem. Eng. Sci. Chemical engineering science* **1985**, *40* (8), 1527–1531, [10.1016/0009-2509\(85\)80094-4](https://doi.org/10.1016/0009-2509(85)80094-4).
41. Mirčeski, V.; Komorsky-Lovrić, S.; Lovrić, M. *Square-wave voltammetry: Theory and application*; Berlin: Springer; Berlin, 2007, [10.1007/978-3-540-73740-7](https://doi.org/10.1007/978-3-540-73740-7).
42. Skinner, J. F.; Glasel, A.; Hsu, L. C.; Funt, B. L. Rotating ring disk electrode study of the hydrogen peroxide oxidation of Fe-(II) and Cu-(I) in hydrochloric acid. *J. Electrochem. Soc. Journal of The Electrochemical Society* **1980**, *127* (2), 315, [10.1149/1.2129663](https://doi.org/10.1149/1.2129663).
43. Nicol, M. J. Kinetics of the oxidation of copper-(I) by oxygen in acidic chloride solutions. *S. Afr. J. Chem. South African Journal of Chemistry* **1984**, *37* (3), 77–80.
44. Masarwa, M.; Cohen, H.; Meyerstein, D.; Hickman, D. L.; Bakac, A.; Espenson, J. H. Reactions of low-valent transition-metal complexes with hydrogen peroxide. Are they "Fenton-like" or not? 1. The case of Cu⁺ aq and Cr²⁺ aq. *J. Am. Chem.*

- [Soc. Journal of the American Chemical Society](#) **1988**, *110* (13), 4293–4297, [10.1021/ja00221a031](#).
45. Pham, A. N.; Xing, G.; Miller, C. J.; Waite, T. D. Fenton-like copper redox chemistry revisited: Hydrogen peroxide and superoxide mediation of copper-catalyzed oxidant production. *J. Catal. Journal of catalysis* **2013**, *301*, 54–64, [10.1016/j.jcat.2013.01.025](#).
 46. Song, P.; Fisher, A. C.; Wadhawan, J. D.; Cooper, J. J.; Ward, H. J.; Lawrence, N. S. A mechanistic study of the EC' mechanism—the split wave in cyclic voltammetry and square wave voltammetry. *RSC Adv. RSC advances* **2016**, *6* (74), 70237–70242, [10.1039/C6RA08723J](#).
 47. Evans, D. H. One-electron and two-electron transfers in electrochemistry and homogeneous solution reactions. *Chem. Rev. Chemical Reviews* **2008**, *108* (7), 2113–2144, [10.1021/cr068066l](#).
 48. Datta, D. Two-step electron transfer & disproportionation of simple Cu⁺ ion. *Indian J. Chem.* **1987**, *26A*, 605–606.
 49. O'Sullivan, D. W.; Lee, M.; Noone, B. C.; Heikes, B. G. Henry's Law Constant Determinations for Hydrogen Peroxide, Methyl Hydroperoxide, Hydroxymethyl Hydroperoxide, Ethyl Hydroperoxide, and Peroxyacetic Acid. *J. Phys. Chem. The Journal of Physical Chemistry* **1996**, *100* (8), 3241–3247, [10.1021/jp951168n](#).
 50. Sander, R. Compilation of Henry's law constants (version 4.0) for water as solvent. *Atmos. Chem. Phys.* **2015**, *15*, 4399–4981, [10.5194/acp-15-4399-2015](#).

[Table of Contents Image](#)

[TOC Graphic](#)